ATOMIC ARRANGEMENT OF MERWINITE, Ca₃Mg[SiO₄]₂, AN UNUSUAL DENSE–PACKED STRUCTURE OF GEOPHYSICAL INTEREST

PAUL BRIAN MOORE AND TAKAHARU ARAKI, *The Department of the Geophysical Sciences, The University of Chicago, Chicago, Illinois 60637*

"Tremble, for dire peril walks,
Monstrous acrimony's spurning merwinite's laws"
N. L. Bowen (1940)[1]

ABSTRACT

Merwinite, Ca₃Mg[SiO₄]₂, is an important and persistent phase in petrological systems crucial to mantle and crustal chemistry and to the cement and blast furnance industries. Despite numerous studies on its crystal chemistry, all reports recorded heretofore in the literature are erroneous in various details.

The crystal cell data are: space group $P2_1/a$, a 13.254(21), b 5.293(9), c 9.328(17)Å, β 91.90(15)°, $Z = 4$. The unit formula, Ca₃Mg[SiO₄]₂, constitutes the asymmetric unit of the crystal structure with all atoms in general positions. Solution of the structure proceeded from Patterson and β-general syntheses, and led to $R(hkl) = 0.061$ for 2300 independent reflections.

The atomic arrangement possesses a substructure of pseudo–hexagonal character, whose axes are parallel to [010], [011], and [01$\bar{1}$]. Crystals are often grossly distorted with frequent prismatic development along [011] or [01$\bar{1}$]. Crystals which most closely approximate ideal monoclinic holosymmetry are thick tabular parallel to a {100}, revealing a pseudotrigonal outline. Prominent forms in order of decreasing importance are h {21$\bar{1}$}, f {011}, c {001} and g {101}. The cleavage is good parallel to {100}.

The atomic structure is an extreme example of dense–packing where both O^{2-} and Ca^{2+} ions comprise the dense–packed layers. The [MgO₆] octahedra are linked at every corner by [SiO₄] tetrahedra, defining a "pinwheel" of $\bar{3}m$ point pseudosymmetry. The pinwheels link indefinitely to form slabs parallel to {100}. The geometrically idealized merwinite arrangement includes Ca(1) in 12–coordination by O^{2-} anions defining a polyhedron with point pseudosymmetry $\bar{3}m$, and Ca(2) and Ca(3) each in 10–coordination whose polyhedra have point pseudosymmetry $3m$. Its idealized arrangement is the glaserite structure type. Distortions in the real structure lead to lower coordination numbers, between 8 and 9 for Ca^{2+}. The structure is also related to other numerous Ca₂[SiO₄] and alkali sulfate polymorphs.

On the basis of the atomic arrangement, it is proposed that merwinite should be an important high-pressure structure type.

[1] Bowen's mnemonic jingle with *merwinite* substituted in proper sequence for *mercy*. The order of the ten minerals as regards their production at rising temperature is tremolite–forsterite–diopside–periclase–wollastonite–monticellite–åkermanite–spurrite–merwinite–larnite.

Introduction

Merwinite, $Ca_3Mg[SiO_4]_2$, was first described by Larsen and Foshag (1921) as a major constituent of a high grade metamorphic contact rock from the famous quarries at Crestmore, near Riverside, California. It occurred in ton quantities intimately associated with gehlenite, spurrite, monticellite (= "mineral A" of the above authors), and more rarely idocrase. Where diopside and wollastonite are abundantly associated with the gehlenite, merwinite was observed to be rare or absent. Tilley (1929) noted its occurrence from Scawt Hill, Co. Antrim, Ireland, where its typical associates include spurrite, gehlenite, and spinel. Since then, numerous localities have been reported in the literature, with merwinite invariably associated with spurrite and gehlenite.

Merwinite is of considerable interest to the cement industries since it is a major component of blast furnace slags and since it does not "fall" or disintegrate in the solid state as do the high temperature $Ca_2[SiO_4]$ polymorphs. Thus, dolomitic limestones are used to inhibit "fall" through the formation of merwinite instead of the high temperature calcium nesosilicates. Phemister *et al.* (1942) outlined a voluminous literature on the subject and presented data on the synthetic merwinite which duplicates the physical and optical characters of the natural material.

Despite the great importance of merwinite and the many crystal–chemical papers on the subject, it became abundantly clear throughout our study that crystal–chemical injustices were bestowed upon the compound. Our crystal cell parameters, with one exception, do not agree with any of the studies of earlier investigators but they do show where the earlier workers went astray. Table 1 cumulates the single crystal investigations recorded in the literature. Bredig (1945) concluded that merwinite is a solid solution, nothing more than $\alpha'-Ca_2[SiO_4]$, which possesses the $\beta-K_2[SO_4]$ structure. From this conclusion, he demonstrated close relationships between his calculated interplanar spacings and the observed data of Phemister *et al.* (1942). Goldschmidt and Rait (1943) suggested that merwinite is isotypic with perovskite. Nurse (1952), in a very detailed review on the $Ca_2[SiO_4]$ polymorphs, presented crystal cell data based on a single crystal study which we offer in Table 1. We shall prove that Nurse had the misfortune of rotating his crystal about the [011]–axis of the true monoclinic cell, and that his parameters are in fact [011], [03$\bar{1}$]/2, and [100] respectively, with triclinic intensity distribution on individual films. Finally, Jahn (1954) noted the compound $Na_3Li[BeF_4]_2$ and suggested isotypy with merwinite, a conclusion we throw into question further on.

– 24 –

TABLE 1. MERWINITE. CRYSTAL CELL PARAMETERS.

	1	2	3	4	5	6
a	13.254(21) Å	9.336	10.72	10.77	6.78	6.52
b	5.293(9)	5.301	9.21	9.20	5.20	9.62
c	9.328(17)	13.286	13.25	13.26	9.20	12.26
β	91.90(15)°	92°8'	~ 91°	91°	–	126°8'
specific gravity	3.150					
density (gm/cm^3)	3.33;3.31	3.32			3.34	
space group	$P2_1/\underline{a}$	$P2_1/c$		?	Pnma	
z	4					
formula		$Ca_3Mg[SiO_4]_2$			$(Ca_{0.75}Mg_{0.25})_2[SiO_4]$	$Na_3Li[BeF_4]_2$

[1]This study. The specific gravity was determined with a pycnometer by Larsen and Foshag (1921). The first calculated density is from the crystal cell, the second from the specific refractive energies of the oxides in Larsen and Berman (1934) using the mean of the indices of refraction determined by Larsen and Foshag (1921).

[2]Yamaguchi, et al. (1967).

[3]Computation of $[011]$, $\frac{1}{2}[03\bar{1}]$ and $[100]$ in that order based on the cell in 1.

[4]Nurse (1952). Note excellent agreement with computations in 3.

[5]Bredig (1945), with axes interchanged. The space group is based on his proposed isotypy with $\beta -K_2[SO_4]$. Note approximate relationship to cell in our study.

[6]Jahn (1954) on low temperature modification.

EXPERIMENTAL

Preparation of the crystals

Single crystals of merwinite for this study were synthesized by Dr. J. K. Robertson and Mr. W. L. Huang, following experimental results by Franz (1965) in the system $CaO-MgO-SiO_2-CO_2-H_2O$. The starting material, prepared by G. W. Franz, consisted of 7 percent calcite, 63 percent portlandite, and 30 percent forsterite. This material was reacted for 7½ days in standard cold seal pressure vessels, with excess water, at 850°C and 1 kbar. The phase relationships at 1 kbar were illustrated by Franz and Wyllie (1967, Fig. 9.14). Merwinite crystals were picked from a assemblage of merwinite plus periclase plus quenched liquid. Virtual identity of this synthetic merwinite with natural Crestmore material was established on the basis of rotation and Weissenberg single crystal photography on both synthetic and natural samples. On the basis of the phase equilibria studies and on the evidence of the structure analysis presented herein, the ideal composition $Ca_3Mg[SiO_4]_2$ was elected.

Morphological character of synthetic merwinite

Natural euhedral crystals of merwinite are extremely rare and invariably rounded and pitted, often showing polysynthetic twinning according to two laws. The synthetic crystals, however, were well–developed, rarely twinned, euhedral, and possessed brilliant facets. Observations on several dozen crystals, which ranged from 0.05 to 1.0 mm in dimension, revealed fantastic distortions from ideality. Briefly, two kinds of developments were observed and have crucial bearing on relating the true cell to the others reported in the literature. By far the more frequent were prismatic crystals, about three to six times as long as they are thick. The prism axis was subsequently established as [011] or [01$\bar{1}$]. The other, less frequent, development consists of tabular crystals with a distinct pseudotrigonal outline when visualized perpendicular to the

large tabular face. The latter crystals most closely approximate ideal merwinite development. A typical development is featured in Figure 1 and was established by two–circle reflection goniometry applied to six crystals including the prismatic developments suitably re–oriented. The morphological cell was established to conform with the results of the single crystal X–ray study. The crystals are monoclinic holosymmetric (2/m), showing large tabular a {100}; and, in the order of decreasing relative frequency h {21$\bar{1}$}, f {011}, c {001}, and g {101}.

Crystal cell parameters

One of the problems crucial to merwinite crystal chemistry is the true unit cell and crystal system. We submit that all crystal cell data published heretofore are either incomplete or erroneous with the exception of a recent Japanese study. The crystal cell parameters reported in our study were obtained from 0–, 1–, and 2–level Weissenberg photographs about the b–axis and 0–, 1–, and 2–level photographs about the c–axis. The correct orientation of the unique axis was assisted by the morphological investigations and the 2/m point symmetry observed for the tabular crystals. Our crystal cell parameters in Table 1 were obtained by least-squares refinement of indexed powder data in Table 2 which were collected from the synthetic crystals crushed with Si($a = 5.4301$ Å) standard and rolled into a small sphere with rubber cement. The space group, $P2_1/a$, is uniquely determined, and is substantiated from the film and crystal structure data. The correct indexing of the powder lines was facilitated by the three-dimensional single crystal intensity data. All powder data on merwinite in the literature are incomplete, incorrectly indexed, and should be abandoned.
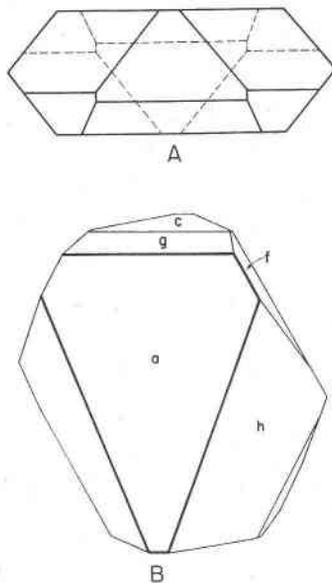

Fig. 1. Synthetic merwinite. Tabular crystal showing the forms c {001}, a {100}, f {011}, g {101}, and h {21$\bar{1}$}. A. Plan. B. Clinographic projection.

25-27

TABLE 2. MERWINITE. POWDER DATA.

(Fe/Mn radiation, 114.6 mm camera diameter, Si(a=5.4301 Å) internal).

I/I_o	d(obs)	d(calc)	hkl		I/I_o	d(obs)	d(calc)	hkl
2	9.27	9.32	001		1	1.821	1.819	$\bar{4}14$
2	6.60	6.62	200		1	1.757	1.752	$\bar{5}22$
3	4.630	4.603	011		1	1.729	1.728	$\bar{6}13$
2	3.865	3.873	$\bar{2}02$		3	1.636	1.656	800
2	3.740	3.751	211		1	1.612	1.610	331
3	3.310	3.312	400				1.606	$\bar{6}22$
3	3.128	3.160	311		2	1.578	1.566	$\bar{8}11$
2	3.032	3.062	212		1	1.554	1.554	006
4	2.749	2.743	$\bar{4}02$	brd	3	1.534	1.544	802
10	2.672	2.709	$\bar{4}11$				1.534	033
		2.680	013		2	1.488	1.500	$\bar{2}33$
3	2.650	2.646	020		2	1.431	1.427	$\bar{8}13$
1	2.456	2.460	213		1	1.407	1.401	$\bar{4}33$
3	2.326	2.321	$\bar{3}13$		1	1.392	1.397	$\bar{6}15$
3	2.311	2.313	$\bar{5}11$				1.391	813
2	2.273	2.280	511		2	1.341	1.340	026
		2.261	122		1	1.338	1.329	804
4	2.213	2.222	$\bar{2}04$		1	1.323	1.323	040
3	2.169	2.176	204				1.321	$\bar{2}26$
2	2.103	2.116	$\bar{1}14$					
2	2.059	2.055	$\bar{3}22$		1	1.233		
3	2.024	2.027	322		2	1.229		
		2.021	$\bar{6}02$		2	1.221		
4	1.909	1.905	$\bar{4}22$		1	1.194		
3	1.875	1.877	404		1	1.190		

All prismatic crystals rotated about the prism axis revealed a triclinic "pseudo-orthohexagonal" geometry. This prism axis corresponds to either the [011] or the [01$\bar{1}$] directions of the true merwinite cell. We shall discuss, further on, that the merwinite structure has a profound pseudohexagonal geometry with the pseudohexagonal axes corresponding to [011], [010], and [01$\bar{1}$]. Accordingly, crystals during their growth frequently tend to distort along the [011] and [01$\bar{1}$] directions, resulting in a pronounced prismatic development which masks the ideal monoclinic $2/m$ symmetry.

We conclude that Nurse (1952) in fact rotated his crystal about the [011]–axis, which for the 0–level projection, reveals the [100]* and [03$\bar{1}$]* axes. The [03$\bar{1}$] axis is the pseudo–orthohexagonal equivalent of [011]. Such a relationship can be readily seen in Figure 2 which reveals what we believe is the Nurse cell referred to the true cell. We note that $[011] = \sqrt{b^2 + c^2} = 10.72$ Å and $[03\bar{1}] = \sqrt{(3b)^2 + c^2} = 18.42$ Å. The angle $[011] \measuredangle [03\bar{1}] = \arctan (c/b) + \arctan (c/3b) = 90°52'$, which deviates only slightly from orthogonality. Setting $[011] = c'$, $[100] = a'$ and $[03\bar{1}] = b'$, the nodal points of the true cell embedded in the Nurse cell in Figure 2 occur at 0, 0; 0, 1/4; 0, 1/2; 0, 3/4 in the a', b' plane. For the zero–level photograph about [011], the systematic absences are $h'k'0$, $k' = 4n$; $h'00$, $h' = 2n$. Agreement with his data in Table 1 is excellent and requires only a halving of the computed [03$\bar{1}$] value
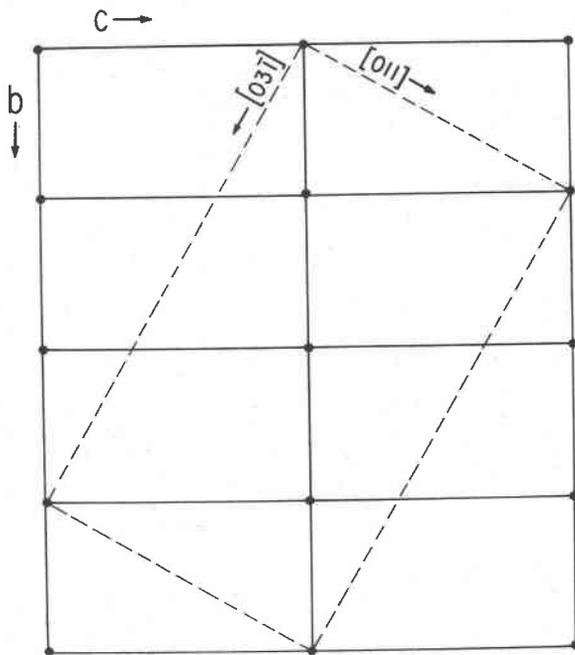
Fig. 2. Merwinite cell down the x^* -axis. The [011] and [03$\bar{1}$] axes define a pseudo–orthohexagonal cell constituted of four primitive cells.

obtained in our study. It is not fully understood how Nurse arrived at monoclinic symmetry for merwinite since the photographs about [011] would reveal triclinic intensity distributions both on the rotation photograph and in the Weissenberg projection.

We examine the cell data of Bredig (1945) and conclude that his incomplete powder data combined with the near–orthogonal character of the crystal in $P2_1/a$ orientation led to a fortuitous calculated agreement with the observed powder lines. Bredig's proposed cell is related to our cell in the following manner: $a_{Br} \sim b$, $b_{Br} \sim c$, $c_{Br} \sim a/2$. Although merwinite is structurally related to $\beta - K_2[SO_4]$, its relationship is sufficiently remote that isotypy cannot exist.

A recent study by Yamaguchi et al. (1967) led to a correct interpretation of the crystal cell but their structure analysis was incomplete and the resulting arrangement only crudely approximate and incorrect in many features. We mention that the paper was not brought to our attention until completion of this study and the good agreement in crystall cell parameters (Table 1) is gratifying. Their computed density of 3.32 gm/cm³ closely agrees with our results in Table 1, which are 3.33 and 3.31 gm/cm³ for the crystal cell and specific refractive energy calculations respectively. We conclude that the specific gravity of 3.150 determined by pycnometry stated by Larsen and Foshag (1921) is low and may have resulted from the presence of minute bubbles and the presence of less dense phases such as gehlenite, spurrite, etc.

Results of the study of Jahn (1954) on low temperature $Na_3Li [BeF_4]_2$ as a model structure for merwinite cannot be so readily explained on the basis of our cell geometry. Jahn's data in Table 1 cannot be unambiguously reconciled by any orientation of the merwinite cell. Since his $Na_3Li [BeF_4]_2$ crystals of the low-temperature modification were morphologically investigated as well, we feel that his compound represents a structure not related to merwinite. Unfortunately, he did not report a space group nor did he investigate merwinite by single-crystal techniques and we are presently growing crystals of his low-temperature compound for a further investigation. Until then, we submit the argument that Jahn's high-temperature $Na_3Li [BeF_4]_2$—from which he tabulated only powder data—may in fact be isostructural with merwinite whereas the low-temperature modification he described corresponds to a low temperature compositionally equivalent but structurally distinct $Ca_3Mg[SiO_4]_2$, so far not reported in the literature in any readily noticeable fashion. In this regard, it appears worthwhile to investigate the so-called "T" $(Ca_{1.7}Mg_{0.3}SiO_4)$ phase (Schlaudt, 1964) which, in many respects, is compositionally akin to merwinite, but as yet suitable single crystals of that compound have not been grown. Incidentally, the powder data of the "T" phase reported by Schlaudt (1964) are very close to those of Nurse (1952) for bredigite. More work is necessary before these compounds can be well–understood.

Structure analysis: Experimental details

A superior, nearly equant, single crystal of synthetic merwinite measuring *ca.* 0.08 mm in mean dimension was selected for study and mounted with the spindle parallel to the *b*–axis. 3600 reflections were collected on a PAILRED automated diffractometer representing the $k = 0$– to 8–levels and utilizing graphite monochromator, Mo radiation, half-angle scans of 1.8° and scan rates of 2.5°/minute with 20 second background counting times on each side of the peak maximum. The hard crystal proved a very good scatterer and we selected $(2\Theta)_{max} = 90°$.

Reduction of the data by standard procedures led to $|F(obs)|$, of which 2300 independent reflections were each greater than three times their background errors and were the only ones accepted for the ensuing analyses and refinements. Absorption correction was unnecessary on account of the small crystal size and the low linear absorption coefficient of 28.8 cm^{-1}. Symmetry equivalent reflections were averaged.

<center>ANALYSIS OF THE STRUCTURE</center>

Solution of the atomic arrangement

The detailed solution of the merwinite atomic arrangement proceeded from the Patterson synthesis which revealed that all prominent peaks were concentrated on levels close to $v = 0$ and 1/2. Thus, the satellite vectors were embedded among and overlapped with unsymmetrical peaks and straightforward distinction was not possible. A clue in the location of some cations was the presence of high density peaks at 0, 1/2, 1/2; 1/4, 1/2, 1/2; and 1/2, 1/2, 1/2.

An image triangle was chosen on the map which spanned the strong peaks mentioned above. Coincidence of the image on other peaks was traced by parallel shifting and a sensible location of the calcium atoms became apparent. In order to test the correctness of the choice, a trial weighted β–general synthesis (Ramachandran and Srinivasan, 1970) was carried out, revealing three atoms

tentatively ascribed calcium at $x_1 = -0.008$, $y_1 = 0.260$, $z_1 = 0.254$; $x_2 = 0.255$, $y_2 = 0.235$, $z_2 = 0.240$; $x_3 = 0.077$, $y_3 = 0.250$, $z_3 = -0.076$, yielding small shifts from $y = 1/4$ in their coordinates. Three additional sharp peaks and three feeble peaks were disclosed on the map. Interpretation of the peaks concluded that two were Si atoms and one a Ca atom, with the Mg atom replacing the first coordinate set in the trial synthesis. The three feeble peaks were ascribed to oxygen atoms. Subsequent β-general synthesis with these nine atoms as inputs successfully revealed all remaining oxygen atoms. Two cycles of successive γ'-synthesis located all the atoms more precisely. The $R(hkl) = \Sigma \mid \mid F(\mathrm{obs}) \mid - \mid F(\mathrm{calc}) \mid \mid / \Sigma \mid F(\mathrm{obs}) \mid = 0.33$ for all reflections prior to final synthesis, with arbitrarily chosen scale factor and isotropic thermal vibration parameters.

Refinement

Coordinates thus obtained were used for a full–matrix least–squares atomic parameter refinement based on a local modification of the familiar ORFLS program of Busing, Martin, and Levy (1962) for the IBM 7094 computer. Form factor tables utilized the curves for Ca^+, Mg^+, Si^{2+}, and O^- in MacGillavry and Rieck (1962). The following parameter refinements were performed in their proper sequence: scale factor; scale factor and atomic coordinates (three cycles); isotropic thermal vibration parameters; and scale factor, atomic coordinate parameters, and isotropic thermal vibration parameters. Convergence was assured at $R(hkl) = 0.061$, with all reflections of equal weight. The independent data: parameter ratio of 40:1, uniform isotropic thermal vibration parameters typical for the ionic species, and low estimated standard errors ($\pm$ 0.004 Å) for the oxygen atoms attest to a well-refined structure whose arrangement can be assessed with considerable definiteness.

Final atomic coordinates and isotropic thermal vibration parameters appear in Table 3. Table 4 presents the $\mid F(\mathrm{obs}) \mid - F(\mathrm{calc})$ data[1].

Details of the Atomic Arrangement

Topology of the closed-packed layers

On account of the short b-axis repeat, it would appear most propitious to project the structure down this axis. Such a projection is featured in Figure 3 as a spoke diagram. It reveals a hopeless clutter of atomic distributions and reveals little valuable information about the principles behind the merwinite arrangement.

The most appropriate projection was suggested by the $0kl$ reflections on a Weissenberg photograph. Figure 4 features the reciprocal net of the b^*c^* plane which reveals a profound substructure possessing a pesudo–hexagonal outline. Define $(a_1^*)_s$, $(a_2^*)_s$ and $(\gamma^*)_s$ as the sub-

---

[1] To obtain a copy of this material, order NAPS Document Number 01860. The present address is National Auxiliary Publications Service of the A.S.I.S., c/o CCM Information Corporation, 866 Third Avenue, New York, New York 10022, and price $2.00 for microfiche or $5.00 for photocopies, payable in advance to CCMIC-NAPS. Check a recent issue of the journal for current address and price.

TABLE 3. MERWINITE. ATOMIC COORDINATES AND ISOTROPIC THERMAL VIBRATION PARAMETERS.
(Estimated standard errors in parentheses refer to the last digit).

Atom	$\underline{x}$	$\underline{y}$	$\underline{z}$	$\underline{B}$ $(Å^2)$
Ca(1)	0.2563(1)	0.1789(2)	0.2234(1)	0.70(1)
Ca(2)	.0811(1)	.2271(2)	- .0753(1)	.66(1)
Ca(3)	.0978(1)	.7333(2)	.4254(1)	.73(1)
Mg	.0043(1)	.2566(3)	.2535(2)	.42(2)
Si(1)	.1326(1)	.2293(2)	.6008(1)	.19(2)
Si(2)	.1412(1)	.7280(2)	.0931(1)	.18(2)
O(1)	.0740(3)	.2123(7)	.4450(4)	1.04(5)
O(2)	.0632(3)	.4193(7)	.6937(4)	.96(5)
O(3)	.1253(3)	- .0475(7)	.6773(4)	.76(4)
O(4)	.2414(3)	.3618(7)	.5940(4)	.91(5)
O(5)	.0768(3)	.7064(7)	- .0591(4)	.87(4)
O(6)	.2548(3)	.8130(7)	.0683(4)	.82(4)
O(7)	.1266(3)	.4726(7)	.1853(4)	.74(4)
O(8)	.0832(3)	- .0424(7)	.1751(4)	.84(4)

structure reciprocal cell. Evidently, $(a_1{}^*)_s = 2b^* = 0.3774$ Å^{-1} and $(a_2{}^*)_s = b^* + 3c^* = 0.3726$ Å^{-1} with $(a_1{}^*)_s \approx (a_2{}^*)_s = 0.3750$ Å^{-1} as an average. Furthermore, $(\gamma^*)_s = 90.00°$-Arctan $(b^*/3c^*) = 59°35' \sim 60.0°$. This defines a pseudo-hexagonal plane cell, with $a_1 = 3.08$ Å. Such a value is a typical octahedral edge distance for [MgO$_6$]. We concluded that the projection down the a^*–axis was the best approach to the structure details and, accordingly, slabs of this projection were dissected in detail.

The key to the structure is a slab of [MgO$_6$] octahedra and [SiO$_4$] tetrahedra which define an hexagonal close-packed (. . . AB . . .) block. The [MgO$_6$] octahedron shares each corner with the [SiO$_4$] tetrahedron, defining a "pinwheel" of polyhedra with point pseudosymmetry $\bar{3}$ $2/m$. Such an arrangement is further polymerized to form the undulating connected slab of polyhedra. Figure 5 reveals the actual structure with its true distortions, but we shall find it more efficaceous to refer to Figure 6 which presents the topologically equivalent and geometrically idealized arrangement. *The most noteworthy feature of the merwinite structure is the presence of mixed cations and anions in the A and B equivalent layers.* The A (and B) layer consists of $2Ca^{2+} + 6O^{2-}$ in a given unit cell slab. Their locations are featured in Figures 5 and 6, the latter representing a visually more accessible construction. The Mg

atoms central to the hexagonal close-packed block are located at $x \sim$ 0, 1/2. To understand the nature of the Ca–O coordination polyhedra it is necessary to examine the close-packed slabs sandwiched in at $x \sim 1/4, 3/4$.

The basis of the slab at $x \sim 1/4$ is shown as the geometrical ideal in Figure 7 which also reveals the sandwiching $A-$ and B–layers above and below. This slab and the B–layer are drawn as triangular tessellations. In the unit cell, the slab consists of 2 Ca^{2+} + 4 O^{2-} ions. Since this slab is *not* geometrically close-packed with respect to the $A-$ and B–layers we define it as the "P" layer. Its tessellation is related to the

A = B = Ca(2)+Ca(3)+O(l)+O(2)+O(3)+O(5)+O(7)+O(8)
P = 2Ca(l) + 2 O(4) + 2 O(6)
Mg = 2Mg
Si = Si(l) + Si(2)
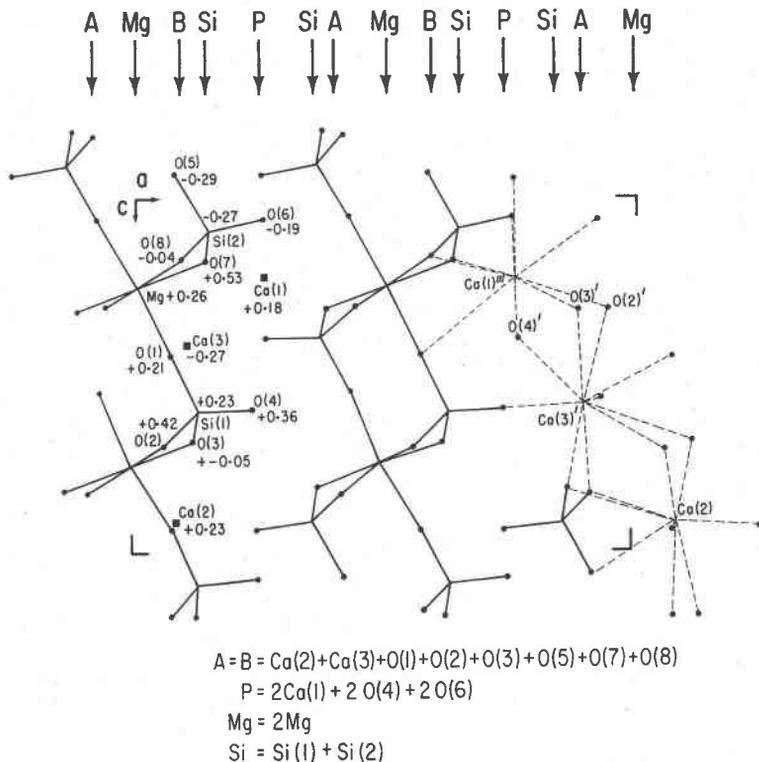
FIG. 3. Spoke diagram of the merwinite structure down the b-axis. Labelling of atoms conforms to Table 3. The [SiO$_4$] and [MgO$_6$] slabs are shown at $a \sim 0$, 1/2 and these slabs are parallel to {100}. The Ca–O bonds are dashed. Locations of the $A-$ and B–dense–packed layers, the P–layer, and the Mg and Si atoms along the a–axis are indicated above. Their atomic constituencies in a given layer in the cell are listed below. Heights at atoms are in fractional coordinates along the y-direction.
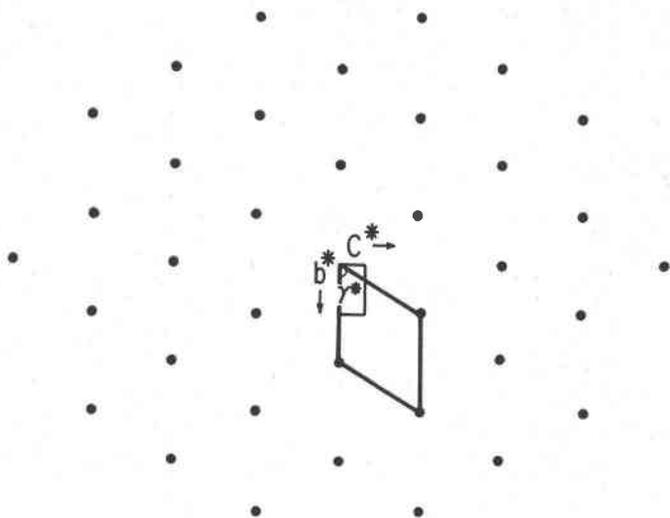
Fig. 4. The b^*c^* reciprocal net in merwinite showing the profound hexagonal substructure in the $0kl$ plane. The pseudo–hexagonal subcell is shown as related to the true reciprocal cell.

B–layer by a 30° rotation of the latter, with a dilation of $(1 + \sqrt{3})/2$ times the B–layer edge. Naturally, its relationship to the overlying A–layer is automatically defined.

We can now interpret the Ca–O coordination polyhedra. For the geometrical ideals, Ca(2) and Ca(3) are components of the A– and B–layers. Using the coordinates in Table 3 as a basis, Ca(2) and Ca(3) in the B–layer are each coordinated to 3 O^{2-} ions in the A–layer below, 6 O^{2-} ions in the plane of the B–layer and 1 O^{2-} ion in the P–layer above. Thus, the ideal coordination numbers for Ca(2) and Ca(3) are 10. The ideal point pseudosymmetry of the resulting polyhedra is 3 mm. The Ca(1) ion, which is situated in the plane of the P–layer, coordinates to 3 O^{2-} in the B–layer below, 3 O^{2-} in the A–layer above and 6 O^{2-} in the plane of the P–layer, resulting in a 12-coordinated polyhedron with ideal point pseudosymmetry $\bar{3}m$. The disposition of anions about the Ca(1), Ca(2), and Ca(3) ions is shown idealized in Figure 8. Included are the interatomic distances found in the actual structure.

The stackings of the A–, B– and P–layers are perpendicular to the a^* ($\sim a$, on account of near-orthogonality) direction and the distribution of cations and anions along the a–axis are shown in Figure 3. The layer sequence is ... $ABPABP$ ..., which involves six layers within the a–axis repeat. Thus, $13.3/6 \sim 2.22$ Å is the average layer separation, a very dense–packed arrangement indeed.
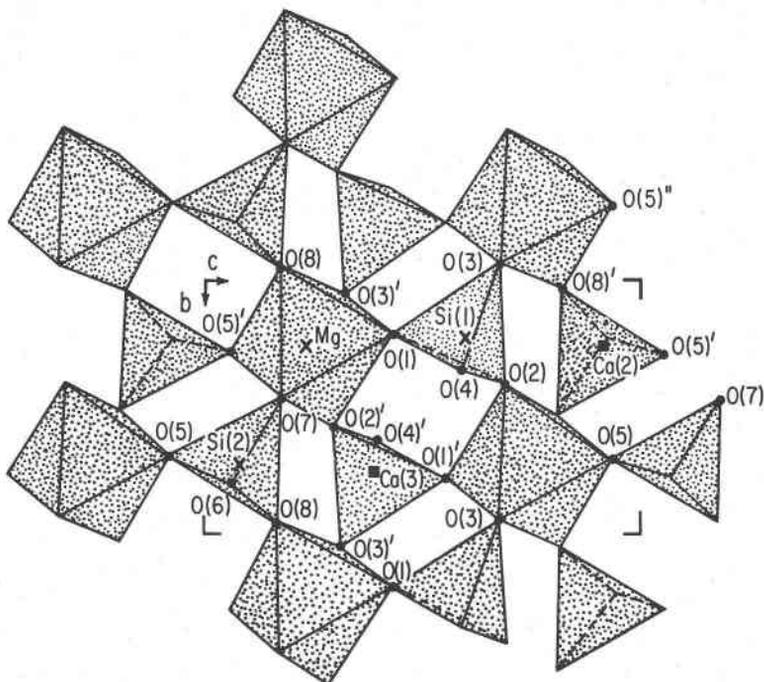
FIG. 5. Polyhedral diagram of a slab of [MgO$_6$] octahedra and [SiO$_4$] tetrahedra down the x^*–axis. Atom positions conform to Table 3.

It is necessary to remark here that the distribution of bonds in the plane normal to the a^*–axis is quite isotropic and does not explain the perfect [010] cleavage observed by Larsen and Foshag (1921). Accordingly, we examined the natural grain during X-ray orientation and discovered that the plane of good cleavage is {100}. This observation agrees well with the expected preferential cleavage parallel to the plane of the dense-packed slabs and not in a direction where Mg–O–Si bonds would be broken. Tilley (1929) observed that merwinite from Scawt Hill is tabular parallel to {010} which agrees with our determination of tabular development parallel to the {100} plane, and suggests that misorientation in the earlier literature may have resulted from the near-orthogonal character of the crystal cell.

The topological and geometrical relationship of the merwinite structure to the Ca$_2$[SiO$_4$] polymorphs and the alkali sulfates, especially glaserite to which it is closely related, is a fascinating and intricate study. Since the literature on these compounds is so enormous, no justice can be allotted to this more general problem in the present ac-

count and one of us (P.B.M.) shall offer the general structural principles among these compounds in a forthcoming article.

Individual polyhedral interatomic distances

The hexagonal pseudosymmetry of the merwinite arrangement is degraded by the misfit of the *P*–layers with the *A*– and *B*–layers resulting from distortions in polyhedral distances leading to symmetry belonging only to the monoclinic system. Accordingly, the idealized coordinations of oxygen about the calcium ions in Figure 8 must be assessed on the basis of computed interatomic distances for the real crystal. For Ca(1), eight Ca–O distances lie between 2.30 and 2.85 Å. The remaining four distances are greater than 3.26 Å. We shall arbitrarily accept Ca(1) [8] as the coordination. In Ca(2), nine distances range between 2.23 and 2.80 Å, with the remaining distance at 3.31 Å. Thus, we accept Ca(2) [9]. In Ca(3), eight distances are between 2.25
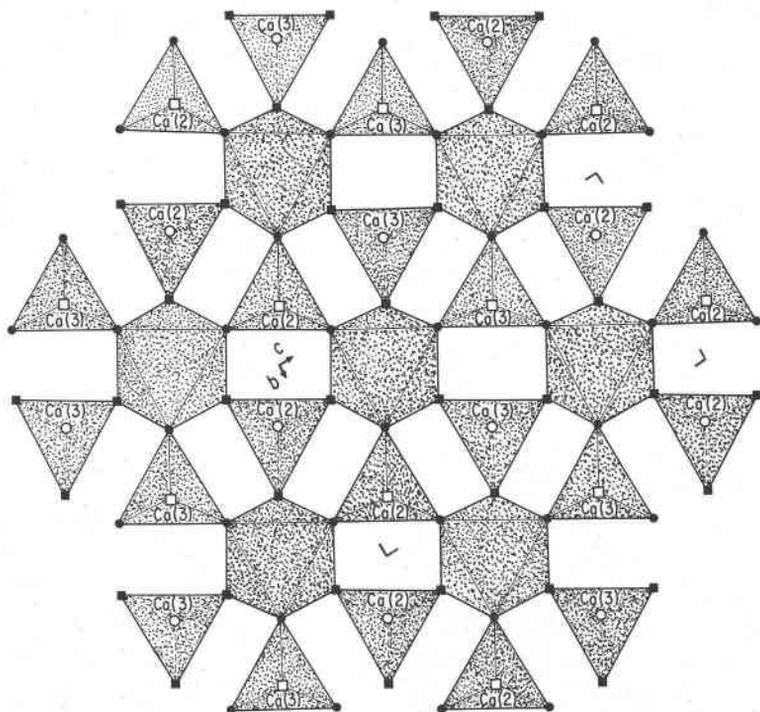

FIG. 6. Geometrically idealized arrangement of the [MgO$_6$] octahedra and [SiO$_4$] tetrahedra. The solid squares are the anions and the open squares the cations in the *A*–layer, and the solid disks are the anions and the open disks the cations in the *B*–layer.
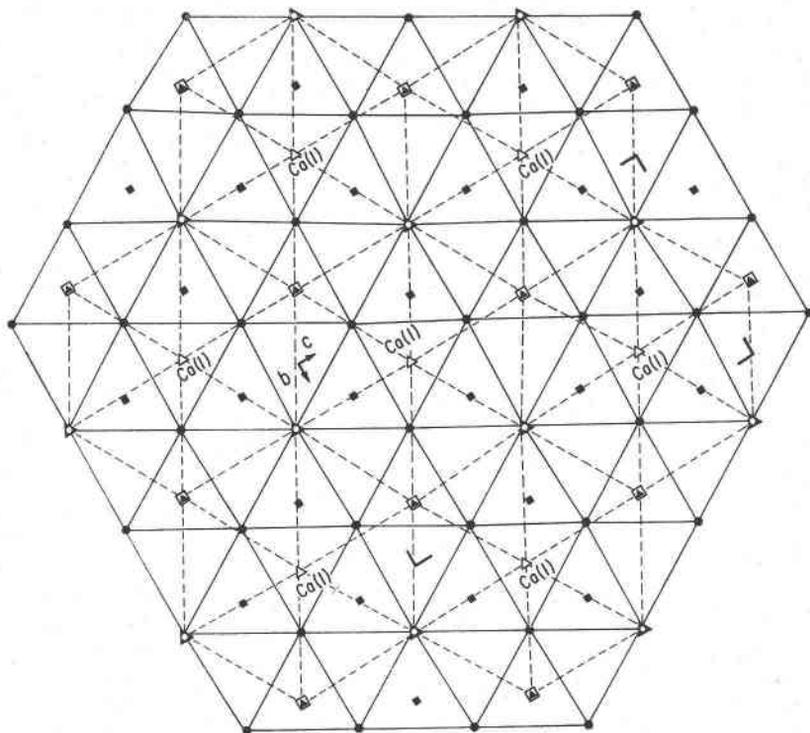
FIG. 7. Idealized merwinite slab at $x \sim 1/4$. The B–layer is shown as a trangular tessellation of solid lines and the P–layer as a tessellation of dashed lines. Solid and open squares are anions and cations in the A-layer above ($x \sim$ 0.4), solid and open disks in the B-layer below ($x \sim 0.1$), and solid and open triangles the cations and anions in the P–layers at $x \sim 1/4$.
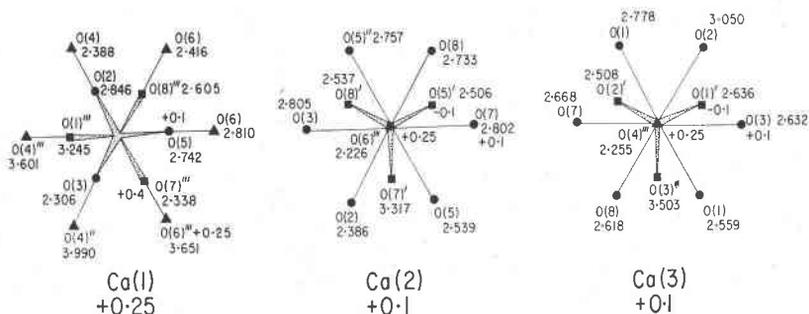

FIG. 8. Idealized coordination polyhedra about Ca(1), Ca(2), and Ca(3). Triangles, squares, and disks correspond to heights of anions conformable to Figure 7. Labelling of atomic positions conform to Table 3. Actual Ca–O interatomic distances are presented.

TABLE 5. MERWINITE. ELECTROSTATIC VALENCE BALANCES (Σ)
OF CATIONS ABOUT ANIONS.

		Σ_a^1	Σ_b^2
O(1)	Si(1) + Mg + 3Ca(3)	2.08	1.93
O(2)	Si(1) + Mg + Ca(1) + Ca(2) + Ca(3)	2.06	1.90
O(3)	Si(1) + Mg + Ca(1) + Ca(2) + Ca(3)	2.06	1.90
O(4)	Si(1) + Ca(1) + Ca(3)	1.50	1.37
O(5)	Si(2) + Mg + Ca(1) + 3Ca(2)	2.25	2.10
O(6)	Si(2) + 2Ca(1) + Ca(2)	1.72	1.53
O(7)	Si(2) + Mg + Ca(1) + Ca(2) + Ca(3)	2.06	1.90
O(8)	Si(2) + Mg + Ca(1) + 2Ca(2) + Ca(3)	2.28	2.10
	Sum	16.01	14.73

[1]Model with Ca(1)[8], Ca(2)[9], Ca(3)[8]

[2]Model with Ca(1)[12], Ca(2)[10], Ca(3)[10]

and 2.78 Å, with the two remaining distances greater than 3.04 Å and we assign Ca(3)[8] for this position.

Further assistance in assigning coordination numbers is the electrostatic valence balance (Σ) of cations about anions. The sums of the individual ζ–values should balance the total charge if the correct coordination numbers are assigned. Utilizing $Si^{[4]}$, $Mg^{[6]}$, $Ca(1)^{[8]}$, $Ca(2)^{[9]}$, and $Ca(3)^{[8]}$, we arrive at the computation in Table 5. This value is ideally neutral, based on the computation of eight nonequivalent oxygen atoms. We conclude that the coordination numbers ascribed to the $[CaO_{\leq 9}]$ polyhedra are "good" values and that the cutoff of the remaining long Ca–O distances is substantiated. Computation based on the "ideal" model results in considerable undersaturation of anions by the cations: -1.26 e.s.u. It is evident that the coordination numbers selected for Ca in this study are in closer agreement to "true" coordination numbers than those for the ideal model.

The Si–O and Mg–O polyhedral distances and their averages are listed in Table 6. The influence of the "soft" $[CaO_{\leq 9}]$ polyhedra which share edges and faces with $[SiO_4]$ and $[MgO_6]$ is considered negligible. It will be noted that the two undersaturated anions, O(4) with $\Sigma = 1.50$ and O(6) with $\Sigma = 1.72$, are associated only with the $[SiO_4]$ and $[CaO_{\leq 9}]$ polyhedra and are the shortest distances observed for these polyhedra.

TABLE 6. MERWINITE $[MgO_6]$ and $[SiO_4]$ POLYHEDRAL INTERATOMIC DISTANCES. (Estimated standard errors, which also apply to Fig. 8, are Me-O$\pm$0.004Å and O-O $\pm$0.006Å based on oxygen e.s.d.'s in Table 3).

Mg		Si(1)		Si(2)	
Mg-O(1)	1.995 Å	Si(1)-O(4)	1.609	Si(2)-O(6)	1.599
-O(2)'	2.003	-O(1)	1.626	-O(7)	1.615
-O(8)	2.047	-O(2)	1.632	-O(5)	1.635
-O(5)'	2.084	-O(3)	1.632	-O(8)	1.641
-O(7)	2.102	Average	1.625	Average	1.623
-O(3)'	2.163				
Average	2.066 Å				
O(5)'-O(2)'	2.759	O(1)-O(2)	2.572	O(5)-O(8)	2.554
O(7)-O(8)	2.783	O(2)-O(4)	2.592	O(7)-O(8)	2.629
O(7)-O(2)'	2.856	O(2)-O(3)	2.608	O(6)-O(8)	2.633
O(1)-O(8)	2.860	O(1)-O(3)	2.634	O(5)-O(7)	2.655
O(5)'-O(3)'	2.873	O(1)-O(4)	2.699	O(5)-O(6)	2.669
O(1)-O(7)	2.891	O(3)-O(4)	2.784	O(6)-O(7)	2.731
O(1)-O(2)'	2.936	Average	2.648	Average	2.645
O(3)'-O(2)'	2.942				
O(5)'-O(8)	2.946				
O(1)-O(3)'	2.976				
O(5)'-O(7)	3.059				
O(3)'-O(8)	3.172				
Average	2.921				

MERWINITE AS A PHASE OF GEOPHYSICAL INTEREST

Although merwinite has been found naturally only in shallow skarn assemblages, such as at Crestmore, California, its appearance in phase equilibria studies as a persistent high pressure phase adds interest to the species.

Kushiro and Yoder (1964) have established that monticellite + forsterite (s.s.) + åkermanite breaks down to merwinite + forsterite (s.s.) + åkermanite at 8–9 kbar and 1400°C. At around 14 kbar, åker-

manite breaks down resulting in the assemblage merwinite + forsterite (s.s.) + diopside. The authors add that this assemblage persists up to at least 38 kbar at 1500°C. Yoder (1968) investigated the åkermanite stability field in detail and found that between 750°C and 6.3 kbar and 1065°C and 10.2 kbar, åkermanite + gas breaks down into merwinite + diopside + gas. Thus, Yoder concluded that merwinite may be a potentially important mantle mineral in calcium–rich and silica–poor regions. So far, the upper limit of pressure stability for merwinite has not been established; the relative stabilities of merwinite and diopside at pressures higher than 38 kbar is an urgent problem of considerable interest.

Of interest in our discussion are the phases åkermanite, $Ca_2Mg[Si_2O_7]$; α–larnite, $Ca_2[SiO_4]$; forsterite, $Mg_2[SiO_4]$; diopside, $CaMg[Si_2O_6]$; wollastonite, $Ca[SiO_3]$; and merwinite, $Ca_3Mg[SiO_4]_2$. Table 7 lists the anion packing indices ($Å^3/O^{2-}$) computed from cell data at 1 atm. pressure. α–larnite ($V = 24.3$ $Å^3/O^{2-}$) and monticellite ($V = 21.4$ $Å^3/O^{2-}$), which possess the olivine structure, are inefficient arrangements compared with merwinite (20.4 $Å^3/O^{2-}$). Although the olivine structure is hexagonal close–packed, the coordination number for the larger cations is only six. Åkermanite ($V = 22$ $Å^3/O^{2-}$) is not a dense–packed structure and does not conserve volume well. It is clear that these compounds break down to merwinite with increase in pressure since higher cation coordination number is achieved without the sacrifice of anionic dense-packing.

We can appreciate the remarkable packing efficiency of merwinite by analogy with the olivine $\rightarrow$ spinel transition. Ringwood (1970) estimates that the spinels are about 10 percent denser than their olivine counterparts. A rough estimate in terms of α–larnite–forsterite

TABLE 7. ANION PACKING INDICES ($Å^3/O^{2-}$) FOR SOME SILICATES.
(Crystal cell data established at room temperature and 1 atm.)

species	formula	cell volume	O^{2-} in cell	$Å^3/O^{2-}$
α -larnite	$Ca_2[SiO_4]$	389.0 $Å^3$	16	24.3 $Å^3$
åkermanite	$Ca_2Mg[Si_2O_7]$	307.9	14	22.0
monticellite	$CaMg[SiO_4]$	342.1	16	21.4
merwinite	$Ca_3Mg[SiO_4]_2$	654.1	32	20.6
forsterite	$Mg_2[SiO_4]$	294.8	16	18.4
diopside	$CaMg[Si_2O_6]$	437.8	24	18.2
coesite	SiO_2	566.8	32	17.7

"solid solution" of merwinite composition would have $V = 24.3 - 1/4$ $(24.3 - 18.4) = 22.8$ Å^3/O^{2-}. A 10 percent decrease of this volume would result in 20.5 Å^3/O^2, the value of merwinite. A good contender for similar packing efficiency is diopside. Diopside is an approximately cubic close–packed structure, where the Ca^{2+} cations are in 8-fold oxygen coordination, crudely defining a square antiprism. It is difficult to compare the packing efficiency of diopside at Ca:Mg = 3:1 composition with merwinite, but crude estimates of the values suggest that the efficiencies of oxygen packing for the two structures are rather close.

One of the advantages of merwinite—like diopside—which makes its structure such an appealing candidate for a high pressure model structure type is the disposition of the [MgO$_6$] octahedra and the [SiO$_4$] tetrahedra. These polyhedra share only corners with each other so that the violent cation–cation repulsion effects are minimized. Kamb (1968) and Moore and Smith (1970) have advanced the argument of the tendency toward minimization of shared edges between [SiO$_4$] tetrahedra and [MgO$_6$] octahedra for the olivine–spinel transition. It is tempting to suggest that the highly coordinated and relatively compressible [CaO$_{\leq 8}$] polyhedra in combination with the absence of shared edges between small highly charged Mg^{2+} and Si^{4+} cations would assure merwinite of a high limit of pressure stability, limited only by the increase of oxygen coordination about Mg^{2+} and Si^{4+}. To assess this, it is necessary to examine the upper pressure stabilities of diopside and merwinite, information apparently which is not yet available. When diopside breaks down, a possible reaction might be

$$3CaMg[Si_2O_6] \rightleftharpoons Ca_3Mg[SiO_4]_2 + Mg_2[SiO_4] + 3SiO_2$$

diopside	$\rightleftharpoons$	merwinite	+	spinel	+	coesite
328.3 Å^3		163.5		66.3		106.2

$$\underbrace{\hspace{6cm}}$$

$$336.0 \text{ Å}^3$$
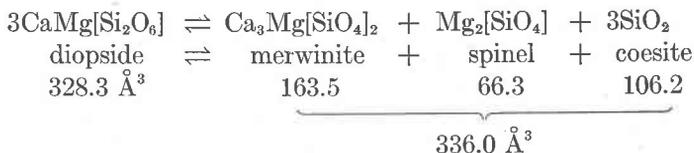
These values are only crude approximations since the compressibilities of the phases have not been taken into account. The difference in volumes is only *ca.* 2.5 percent so no definite conclusions can be drawn, but it does emphasize the importance of such structure types as diopside and merwinite as good models for highly efficient oxygen packings.

Most intriguing is Nature's way of increasing coordination number of cations *without* sacrificing crystallographic dense–packing. In merwinite, this is achieved by mixing of cations and anions in the dense–packed layers. Structures of this kind tend to appear in abundance at high pressures. The hollandite and perovskite structure types are

two such examples. As the crystal radius ratios of the smaller cations to O^{2-} increase with increase in pressure, the tendency of mixed layering should increase. As yet, no systematic survey of such mixed layer arrangements has been made; it promises to be a very fruitful problem.

Finally, we suggest that the merwinite structure type, $X_3M[SiO_4]_2$ may be a good trap for even larger alkaline earth cations and other divalent species. Goldschmidt and Rait (1943) reported the existence of a manganese merwinite, where Mg^{2+} is replaced by Mn^{2+}, but there appears to be little information of the extent of possible substitutions for X. Instructive would be attempts at routine synthesis of compounds with a stoichiometry of merwinite, but with $X = Sr^{2+}, Ba^{2+}, Pb^{2+}$, etc.

REFERENCES

BOWEN, N. L. (1940) Progressive metamorphism of siliceous limestone and dolomite. *J. Geol.* **48**, 225–274.

BREDIG, M. A. (1945) High temperature crystal chemistry of A_mBX_n compounds with particular reference to calcium orthosilicate. *J. Phys. Chem.* **49**, 537–553.

BUSING, W. R., K. O. MARTIN, AND H. A. LEVY (1962) ORFLS, a Fortran crystallographic least-squares program. *U.S. Oak Ridge Nat. Lab. (U.S. Clearinghouse Fed. Sci. Tech. Info.) Rep.* **ORNL-TM-305**.

FRANZ, G. W. (1965) *Melting Relationships in the System* CaO–MgO–SiO_2–CO_2–H_2O: *A Study of Synthetic Kimberlites.* Ph.D. Thesis, Pennsylvania State University.

——, AND P. J. WYLLIE (1967) Experimental studies in the system CaO–MgO–SiO_2–CO_2–H_2O. *In* P. J. Wyllie, ed., *Ultramafic and Related Rocks,* John Wiley and Sons, New York, 323–326.

GOLDSCHMIDT, H. J., AND J. R. RAIT (1943) Silicates of the perovskite type of structure. *Nature*, **152**, 356.

JAHN, W. (1954) Untersuchungen an Silicatmodellen. VI. $Na_3Li[BeF_4]_2$, eine neue Verbindung in ternären System NaF–LiF–BeF_2 und ihre Beziehungen zum Merwinit $Ca_3Mg[SiO_4]_2$. *Z. Anorg. Allgem. Chem.* **277**, 274–286.

KAMB, B. (1968) Structural basis of the olivine-spinel stability relation. *Amer. Mineral.* **53**, 1439–1455.

KUSHIRO, I., AND H. S. YODER, JR. (1964) Breakdown of monticellite and akermanite at high pressures. *Carnegie Inst. Geophys. Lab. Rep.* **1963–1974**, 81–83.

LARSEN, E. S., AND H. BERMAN (1934) The microscopic determination of non-opaque minerals. *U.S. Geol. Surv, Bull.* **848**, 30–31.

————, AND W. F. FOSHAG (1921) Merwinite, a new calcium magnesium orthosilicate from Crestmore, California. *Amer. Mineral.* **6**, 143–148.

MACGILLAVRY, C. H., AND G. D. RIECK (1962) *International Tables for X-ray Crystallography, Vol.* **3**, The Kynoch Press, Birmingham, England.

MOORE, P. B., AND J. V. SMITH (1970) Crystal structure of β–Mg_2SiO_4: crystal-chemical and geophysical implications. *Phys. Earth Planet. Interiors,* **3**, 166–177.

NURSE, R. W. (1952) The dicalcium silicate phase. *Proc. 3rd Int. Symp. Chem. Cement,* 56–90.

PHEMISTER, J., R. W. NURSE, AND F. A. BANNISTER (1942) Merwinite as an artificial mineral. *Mineral. Mag.* **26**, 225–231.

RAMACHANDRAN, G. N., AND R. SRINIVASAN (1970) *Fourier Methods in Crystallography.* Wiley–Interscience, New York, 96–119.

RINGWOOD, A. E. (1970) Phase transformations and the constitution of the mantle. *Phys. Earth Planet. Interiors,* **3**, 109–155.

SCHLAUDT, C. M., (1964) *Phase Equilibria and Crystal Chemistry of Cement and Refractory Phases in the System* $CaO–MgO–Al_2O_3–Fe_2O_3–CaF_2–P_2O_5–SiO_2$ Ph.D. Thesis, The Pennsylvania State University.

TILLEY, C. E. (1929) On larnite (calcium orthosilicate, a new mineral) and its associated minerals from the limestone contact zone of Scawt Hill, Co. Antrim. *Mineral. Mag.* **22**, 77–86.

YAMAGUCHI, G., AND K. SUZUKI (1967) Structural analysis of merwinite (in English). *Yogyo Kyokaishi (J. Ceram. Assoc. Jap).* **75**, 220–229.

YODER, H. S., JR. (1968) Akermanite and related melilite-bearing assemblages. *Carnegie Inst. Geophys. Lab. Rep.* **1966–1967**, 471–474.